CellPress

Cancer Cell
Article

EWS-FLI1 Utilizes Divergent Chromatin Remodeling Mechanisms to Directly Activate or Repress Enhancer Elements in Ewing Sarcoma

Nicolò Riggi,[1,2,14] Birgit Knoechel,[1,2,3,4,14] Shawn M. Gillespie,[1,2,5,14] Esther Rheinbay,[1,2] Gaylor Boulay,[1,2] Mario L. Suvà,[1,2] Nikki E. Rossetti,[1] Wannaporn E. Boonseng,[1] Ozgur Oksuz,[1] Edward B. Cook,[1] Aurélie Formey,[6] Anoop Patel,[5,7] Melissa Gymrek,[8,9,10] Vishal Thapar,[11] Vikram Deshpande,[12] David T. Ting,[11] Francis J. Hornicek,[13] G. Petur Nielsen,[12] Ivan Stamenkovic,[6] Martin J. Aryee,[1,2] Bradley E. Bernstein,[1,2,5,15,*] and Miguel N. Rivera[1,2,15,*]

[1]Department of Pathology and Center for Cancer Research, Massachusetts General Hospital and Harvard Medical School, Boston, MA 02114, USA
[2]Broad Institute of MIT and Harvard, Cambridge, MA 02142, USA
[3]Department of Pediatric Oncology, Dana-Farber Cancer Institute, Boston, MA 02115, USA
[4]Division of Hematology/Oncology, Boston Children's Hospital and Harvard Medical School, Boston, MA 02115, USA
[5]Howard Hughes Medical Institute, Chevy Chase, MD 20815, USA
[6]Institute of Pathology, Centre Hospitalier Universitaire Vaudois, Faculty of Biology and Medicine, University of Lausanne, 1011 Lausanne, Switzerland
[7]Department of Neurosurgery, Massachusetts General Hospital and Harvard Medical School, Boston, MA 02114, USA
[8]Whitehead Institute for Biomedical Research, 9 Cambridge Center, Cambridge, MA 02142, USA
[9]Harvard-MIT Division of Health Sciences and Technology, MIT, Cambridge, MA 02139, USA
[10]Program in Medical and Population Genetics, Broad Institute of MIT and Harvard, Cambridge, MA 02142, USA
[11]Cancer Center, Massachusetts General Hospital and Harvard Medical School, Charlestown, MA 02129, USA
[12]Department of Pathology, Massachusetts General Hospital and Harvard Medical School, Boston, MA 02114, USA
[13]Center for Sarcoma and Connective Tissue Oncology, Massachusetts General Hospital and Harvard Medical School, Boston, MA 02114, USA
[14]Co-first author
[15]Co-senior author
*Correspondence: bernstein.bradley@mgh.harvard.edu (B.E.B.), mnrivera@mgh.harvard.edu (M.N.R.)
http://dx.doi.org/10.1016/j.ccell.2014.10.004

SUMMARY

The aberrant transcription factor EWS-FLI1 drives Ewing sarcoma, but its molecular function is not completely understood. We find that EWS-FLI1 reprograms gene regulatory circuits in Ewing sarcoma by directly inducing or repressing enhancers. At GGAA repeat elements, which lack evolutionary conservation and regulatory potential in other cell types, EWS-FLI1 multimers induce chromatin opening and create de novo enhancers that physically interact with target promoters. Conversely, EWS-FLI1 inactivates conserved enhancers containing canonical ETS motifs by displacing wild-type ETS transcription factors. These divergent chromatin-remodeling patterns repress tumor suppressors and mesenchymal lineage regulators while activating oncogenes and potential therapeutic targets, such as the kinase VRK1. Our findings demonstrate how EWS-FLI1 establishes an oncogenic regulatory program governing both tumor survival and differentiation.

INTRODUCTION

Transcriptional regulators, including transcription factors, chromatin modifiers, and histones, are key mediators of proliferation and differentiation in normal development and cancer. Such genes are frequent targets of genetic alterations in tumors and can be important contributors to transformation through the dysregulation of transcriptional programs (Baylin and Jones, 2011;

Significance

Cancer genome studies have identified many alterations in transcriptional regulators that have the potential to promote oncogenic gene expression programs. The impact of such changes is particularly evident in pediatric malignancies, where they may represent the sole event in tumor initiation. In our study, the integrated analysis of chromatin states in Ewing sarcoma reveals that EWS-FLI1 can either serve as a pioneer factor to generate enhancers de novo at repeat elements or repress conserved enhancers by competing with endogenous ETS factors. These data show how a single oncogenic transcription factor can directly orchestrate divergent patterns of chromatin remodeling in cancer and point to mechanisms that may be applicable to other tumors where transcriptional aberrations play a major role.

Lee and Young, 2013). Pediatric tumors offer unique opportunities to study these events in relative isolation because they have stable genetic backgrounds and small numbers of genetic alterations that often involve transcriptional regulators (Kadoch and Crabtree, 2013; Roberts et al., 2000; Schwartzentruber et al., 2012). This is in sharp contrast to most tumors in adults, where the genome-wide analysis of regulatory networks is complicated by many recurrent mutations and genomic instability.

Ewing sarcoma, the second most common bone malignancy in children and young adults, is a prototypical example of a pediatric tumor with a dominant genetic alteration in a transcriptional regulator. Ewing sarcoma is characterized by chromosomal translocations that generate fusions between the *EWS* gene and members of the *ETS* family of transcription factors, by far the most common being *FLI1* (Delattre et al., 1992). The importance of the translocation is further supported by the fact that it occurs in the setting of one of the lowest mutation rates among all cancer types (Lawrence et al., 2013). The EWS-FLI1 oncogenic fusion protein not only constitutes a defining diagnostic feature of Ewing sarcoma but also underlies its pathogenesis. Indeed, several studies have shown EWS-FLI1 to be crucial for the growth and survival of Ewing sarcoma cells and sufficient for the transformation of primary mesenchymal stem cells (Riggi et al., 2005, 2008), a putative cell of origin.

Gene expression studies have shown that the oncogenic properties of EWS-FLI1 are linked to a complex transcriptional program that involves both gene activation and repression (Riggi and Stamenkovic, 2007). The pathways implicated include known mediators of transformation as well as genes involved in cellular differentiation that point to the interruption of normal mesenchymal development. This is consistent with the proposed origin of Ewing sarcoma from mesenchymal stem cells (MSCs) and with experiments showing that EWS-FLI1 can transform these cells and prevent their differentiation into osteogenic and adipogenic fates (Torchia et al., 2003). EWS-FLI1 is therefore capable of eliciting profound changes in gene regulation and reprograms precursor cells to establish a distinct differentiation and oncogenic state.

The mechanisms by which EWS-FLI1 directly regulates target genes are less well understood. EWS-FLI1 binding sites have been described previously (Bilke et al., 2013; Gangwal et al., 2008; Guillon et al., 2009; Patel et al., 2012), but the direct chromatin remodeling events leading to gene activation and repression remain to be fully elucidated. Here we pursued the coordinated analysis of chromatin states at EWS-FLI1 binding sites in Ewing sarcoma primary tumors, cell lines, and precursor pediatric mesenchymal stem cells to characterize the mechanisms by which EWS-FLI1 directly modulates critical transformation and differentiation pathways.

RESULTS

EWS-FLI1 Binds *cis*-Regulatory Elements Shared by Ewing Sarcoma Cell Lines and Primary Tumors

To map EWS-FLI1 and its associated chromatin states, we first identified direct binding sites of endogenous EWS-FLI1 in two well defined Ewing sarcoma cell lines, A673 and SKNMC. This was achieved by chromatin immunoprecipitation sequencing (ChIP-seq) with an antibody directed against the C-terminal portion of FLI1 contained in EWS-FLI1 (endogenous FLI1 is not expressed in either line). 1785 EWS-FLI1 peaks were present in both SKNMC and A673 cells at high significance (p value < 10^{-5}) and were defined as a core set of EWS-FLI1 binding sites for analysis (Figure S1A and Table S1 available online). Ninety percent of these sites were located in intergenic and intronic regions (Figure S1B), and 75% were found to overlap with a recent EWS-FLI1 profiling performed in A673 cells (Bilke et al., 2013). To relate these binding sites to *cis*-regulatory elements and epigenetic states, we mapped key histone modifications, including histone H3 lysine 27 acetylation (H3K27ac), H3 lysine 4 monomethylation (H3K4me1), H3 lysine 4 trimethylation (H3K4me3), and H3 lysine 27 trimethylation (H3K27me3). We found that the majority of EWS-FLI1 binding sites are enriched for H3K4me1, a ubiquitous marker of *cis*-regulatory elements (Figure 1A; 87% of sites have strong signals in both cell lines). However, they display variable levels of H3K27ac, a more specific marker of enhancer activity (Figure 1A; 78% of sites were positive in both cell lines, with a large variation in signal intensity). In contrast, essentially all promoters bound by EWS-FLI1 carry H3K4me3, a mark of transcriptional initiation (Figure 1B; 99% of all bound promoters).

We also mapped these modifications in a set of primary Ewing sarcoma tumors and in MSCs. Chromatin patterns over EWS-FLI1 binding sites were highly concordant between Ewing sarcoma cell lines and the primary tumors (Figure 1A; 87% of sites are concordant for H3K4me1 and 76% for H3K27ac) but distinct from those in mesenchymal stem cells, suggesting that the cell line models are representative of the native tumor environment at these sites (Figure S1C). Genes proximal to EWS-FLI1-bound enhancers include known regulators with critical functions in Ewing sarcoma, such as *CCND1* and *NKX2-2*, as well as many additional targets (Figure 1D). Because EWS-FLI1 has been shown to have both positive and negative effects on gene expression (Riggi and Stamenkovic, 2007), we considered the possibility that EWS-FLI1 regulation might involve Polycomb-mediated repression. However, we observed essentially no overlap between EWS-FLI1 binding sites and H3K27me3, a repressive modification deposited by Polycomb-repressive complexes (Margueron and Reinberg, 2011), in either the cell lines or the primary tumors (Figure 1C; Figure S1D).

EWS-FLI1-Bound Distal Regulatory Elements Are Either Directly Activated or Repressed by the Fusion Protein

To test the functional impact of EWS-FLI1 on enhancer activity directly, we depleted the fusion by small hairpin RNA (shRNA) and measured ensuing changes in the chromatin state. We confirmed an 85% reduction in EWS-FLI1 protein levels and a marked decrease in EWS-FLI1 ChIP-seq signals at binding sites, thus validating the knockdown and the specificity of the ChIP-seq signal for EWS-FLI1 (Figure S2A; ChIP-seq signals decreased more than 1.5-fold at 93% of our core set of 1,785 EWS-FLI1 peaks). EWS-FLI1 depletion significantly altered global enhancer patterns in the tumor cell lines so that they more closely resembled the nontransformed MSCs (Figure S2C). In particular, loss of EWS-FLI1 elicited divergent responses at target sites; some *cis*-regulatory elements displayed marked increases in H3K27ac levels while others displayed

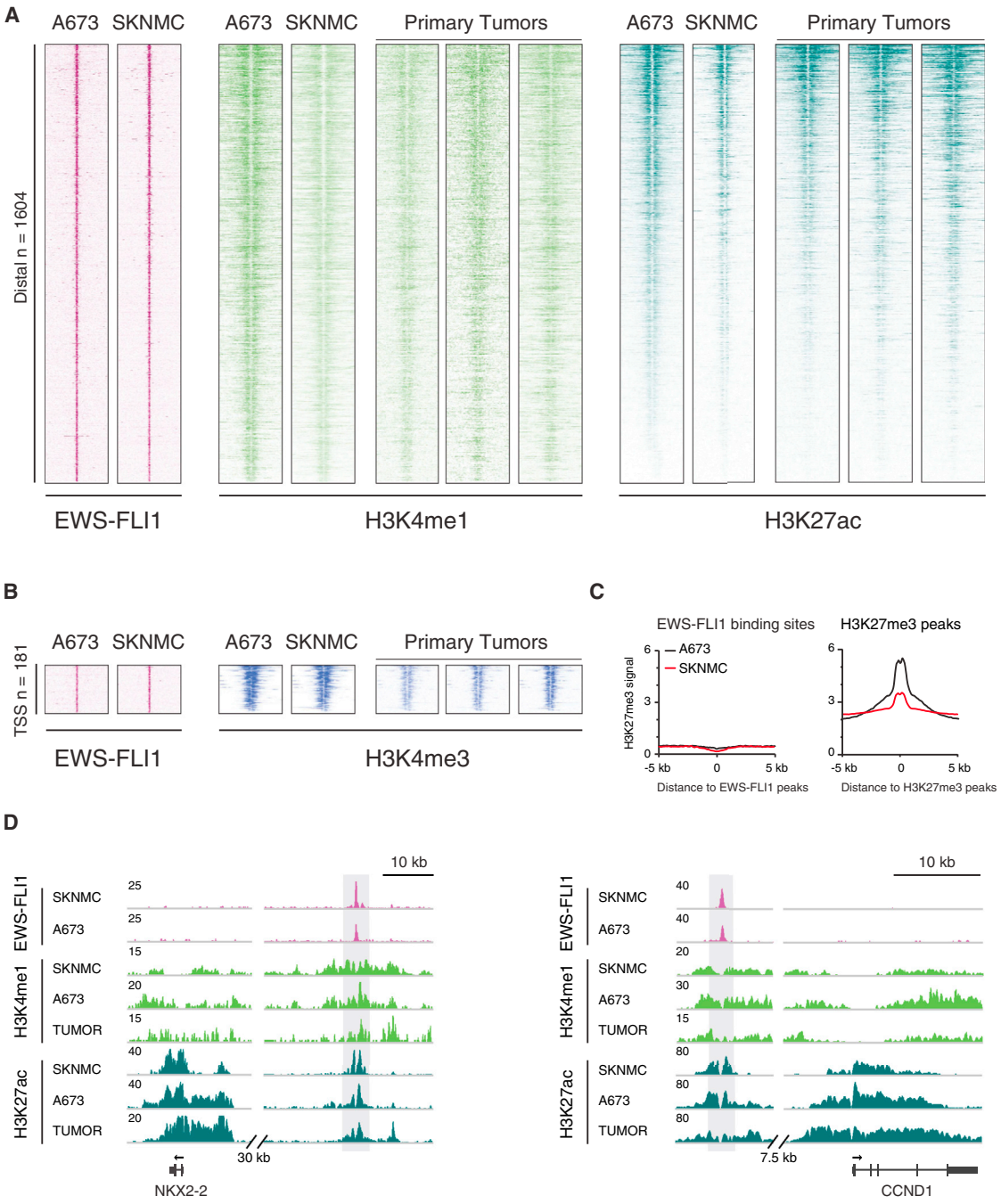

Figure 1. EWS-FLI1 Binds Enhancer Elements in Ewing Sarcoma Cell Lines and Primary Tumors

(A) Heatmaps depicting EWS-FLI1, H3K4me1, and H3K27ac signal intensities for 1604 EWS-FLI1-bound distal regulatory elements. The rows show 10 kb regions, centered on EWS-FLI1 peaks, ranked by overall signal intensities of H3K4me1 and H3K27ac.

(B) Heatmaps depicting EWS-FLI1 and H3K4me3 signals for 181 EWS-FLI1 peaks overlapping with transcriptional start sites (TSS). The rows show 10 kb regions, centered on EWS-FL1 peaks, ranked by overall signal intensities of H3K4me3. EWS-FLI1 binds to enhancers with variable levels of activity, as demonstrated by the presence of the H3K4me1 mark and different levels of the H3K27ac activation mark. In contrast, EWS-FLI1 is primarily found at active promoters.

(C) Composite plots showing average levels of H3K27me3 signals at EWS-FLI1 binding sites (left) compared with genome-wide signals at H3K27me3 peaks (right).

(D) Examples of active distal regulatory elements near known EWS-FLI1 target genes in Ewing sarcoma cell lines (A673 and SKMNC) and a primary tumor. The tracks show EWS-FLI1, H3K27ac, and H3K4me1 signals. EWS-FLI1 binding is highlighted in gray.

See also Figure S1 and Table S1.

equally strong decreases in this marker for enhancer activity (Figure 2A). Classification of binding sites by changes in H3K27ac levels revealed 1,011 EWS-FLI1-activated and 330 EWS-FLI1-repressed loci (fold change >1.5; Figure 2A). Chromatin state changes were evident at 48 hr, indicating that they represent rapid events, and became more pronounced by 96 hr. Results were also highly concordant between the two cell lines (Figure S2B; correlation coefficients of 0.84 at 48 hr and 0.76 at 96 hr). We did not observe changes in H3K27me3 at either class of target elements, ruling out a role for Polycomb repressors in the direct regulation of enhancers by EWS-FLI1 (Figure S2D).

The rapid and robust changes in H3K27ac led us to hypothesize that they might reflect direct interactions between EWS-FLI1 and chromatin remodeling complexes. We focused initially on the acetyltransferase p300, a chromatin regulator implicated in enhancer activity (Visel et al., 2009) and shown previously to interact with EWS-FLI1 to mediate p53 acetylation and apoptosis in response to toxic stress (Ramakrishnan et al., 2004). We used coimmunoprecipitation to confirm that EWS-FLI1 binds p300 in SKNMC cells (Figure S2E). We then mapped p300 binding genome-wide before and after EWS-FLI1 knockdown in the Ewing sarcoma lines. We observed strong p300 signals in 75% of activated EWS-FLI1 binding sites and dynamic changes in p300 occupancy that were closely coordinated with decreases in H3K27ac in activated sites and increases in H3K27ac at repressed sites upon depletion of the translocation (Figure 2A; correlation coefficient 0.75). This suggests that differential effects of EWS-FLI1 on p300 recruitment may underlie its divergent effects on enhancer activity (Figures 2B and 2C).

The Functional Output of EWS-FLI1 Binding Is Determined by the Underlying DNA Sequence

To investigate the mechanistic basis of the divergent effects of EWS-FLI1 on p300 recruitment and enhancer activity, we examined the primary DNA sequence underlying the fusion protein binding sites. De novo motif analysis revealed that the activated and repressed binding sites have distinct sequence determinants. *cis*-Regulatory elements activated by EWS-FLI1 are strongly enriched for GGAA repeats, with 75% of activated sites containing four or more repeats. In contrast, repressed sites contain canonical nonrepetitive ETS motifs in 85% of cases (Figures 2A–2C). Other motifs were present at much lower significance (Figure S2F). GGAA repeats have been implicated previously in Ewing sarcoma on the basis of their association with open chromatin and proximity to some activated genes (Gangwal et al., 2008; Guillon et al., 2009). In biochemical experiments, EWS-FLI1 has been shown to bind these elements as homodimers at optimal lengths of four or more consecutive GGAA repeats (Gangwal et al., 2008; Guillon et al., 2009). Our results show that EWS-FLI1 multimers at GGAA repeats promote the recruitment of p300 to these sites, leading to histone acetylation and an active enhancer state.

GGAA Repeat Enhancers Appear to Be Specific to Ewing Sarcoma

The strong association between the function of EWS-FLI1 and DNA sequence prompted us to investigate whether the two classes of EWS-FLI1 binding sites may have different regulatory activities in other cellular contexts. To this effect, we examined previously published DNase I hypersensitivity data for 112 cell and tissue types (ENCODE Project Consortium, 2012; Thurman et al., 2012). With the exception of the SKNMC Ewing cell line, we did not identify any other cell type in which GGAA repeats activated by EWS-FLI1 show evidence of accessibility or activity (Figure 3A). In contrast, sites repressed by EWS-FLI1 exhibit strong DNase I signals in multiple cell types. We also examined evolutionary conservation at EWS-FLI1 binding sites to explore whether these elements might have selected functions in other cellular or developmental contexts. Remarkably, the conservation of GGAA repeat sites and adjacent sequences is essentially indistinguishable from the genomic background (Figure 3B). In contrast, repressed target sites are highly conserved. Therefore, although repressed target sites have characteristic features of enhancers, our analysis suggests that GGAA repeat activation may be specific to the setting of Ewing sarcoma.

To examine how EWS-FLI1 establishes tumor-specific active enhancers, we turned to primary pediatric MSCs. In contrast to other cell types, where expression of EWS-FLI1 leads to growth arrest and apoptosis, induction of the fusion in MSCs results in transformation and activation of a set of genes that closely recapitulate the Ewing sarcoma phenotype (Riggi et al., 2005, 2010). We therefore infected MSCs with an EWS-FLI1 expression construct (Figures S3A and S3B) and measured consequent changes in DNA accessibility and chromatin state (Figure 3C; Figure S3D). As in other cell types, activated EWS-FLI1 sites have a closed chromatin conformation in primary MSCs, as indicated by the absence of DNase I hypersensitivity and H3K4me1 and H3K27ac signals (Figure 3C; Figure S3C) (ENCODE Project Consortium, 2012; Thurman et al., 2012). However, upon EWS-FLI1 induction, these sites switch to an open chromatin conformation, as indicated by assay of transposase-accessible chromatin (ATAC-seq) chromatin accessibility measurements (Figures 3E and 3F; 77% of activated sites increased more than 1.5-fold). Moreover, EWS-FLI1 induction caused significant increases in both H3K4me1 and H3K27ac at 78% of these sites, resulting in an active enhancer-like pattern analogous to their state in Ewing sarcoma cell lines and primary tissues (Figures 3C and 3E; Figure S3D).

Enhancer priming has been linked to MLL family protein complexes that catalyze H3K4 methylation (Kaikkonen et al., 2013; Smith et al., 2011), leading us to hypothesize that EWS-FLI1 might recruit chromatin remodeling subunits in addition to p300. Consistent with this possibility, we identified interactions between EWS-FLI1 and two components shared by all human MLL complexes, WDR5 and ASH2, by coimmunoprecipitation experiments (Figures S3E and S3F). WDR5 occupancy at activated EWS-FLI1 sites in SKNMC and A673 cells was also detected by ChIP-seq (Figure 3D; Figure S3G; 88% of activated sites). Accordingly, ChIP-seq profiling of MSCs before and after fusion gene induction demonstrated that EWS-FLI1 recruits WDR5 to activated enhancers (Figures 3E and 3F; 63% of activated sites increased more than 1.5-fold). Finally, chromatin conformation analysis showed a direct physical interaction between the *NKX2-2* promoter and the corresponding distal regulatory element in both SKNMC and A673 cells (see Figures 3G and S3H, respectively). A similar high-order chromatin

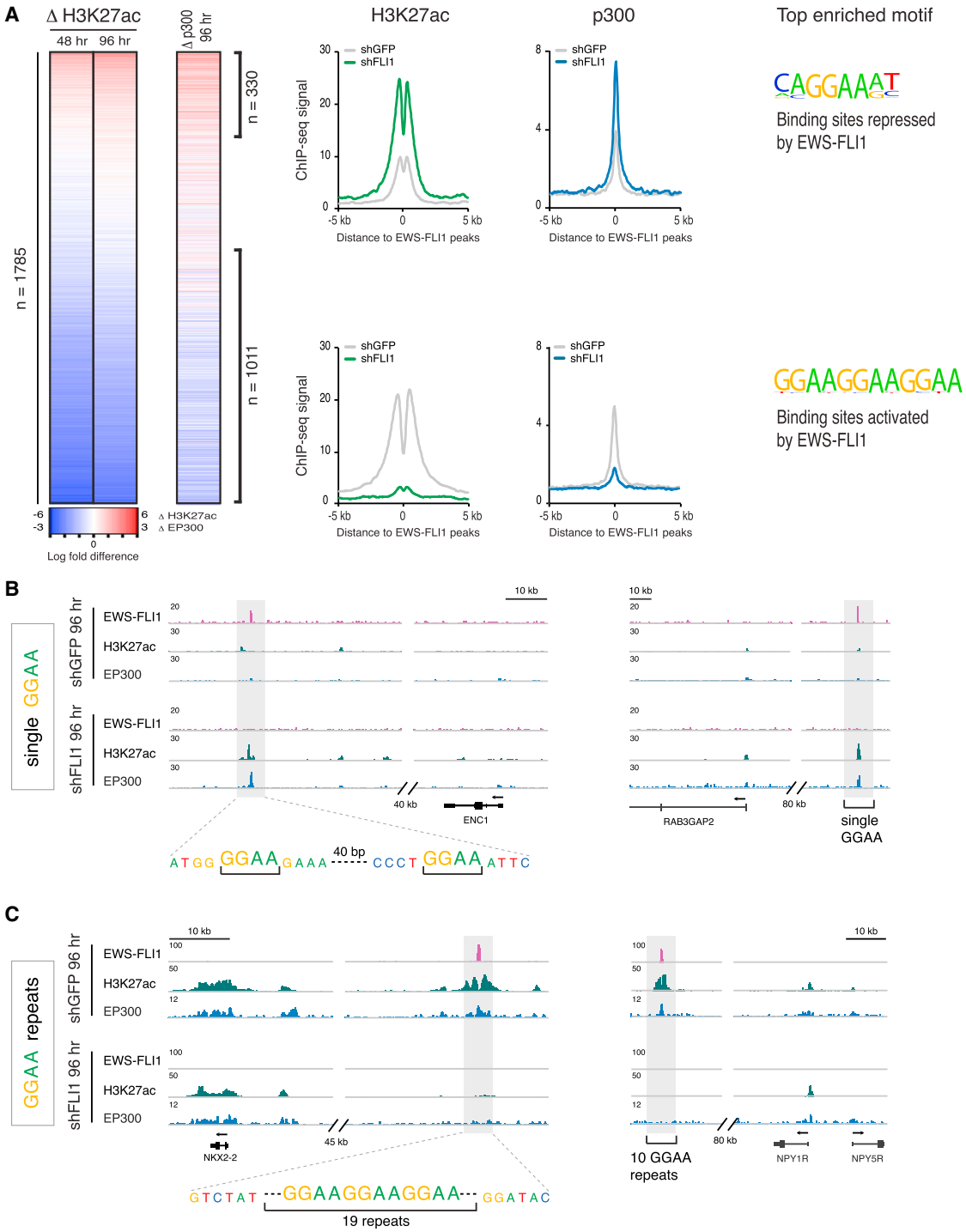

Figure 2. EWS-FLI1 Activates or Represses Enhancers Depending on the Underlying DNA Sequence and Differential Recruitment of p300

(A) Heatmaps (left) and composite plots (center) depicting H3K27ac and p300 signal intensity changes across EWS-FLI1 peaks after EWS-FLI1 knockdown in SKNMC cells at the indicated time points. Binding sites are classified as repressed when EWS-FLI1 depletion results in increased H3K27ac and p300 signals (top, 330 sites, 1.5-fold increase in H3K27ac) or as activated when depletion results in decreases in H3K27ac and p300 (bottom, 1011 sites, 1.5-fold decrease in H3K27ac). Right: de novo motif analysis of repressed peaks shows strong enrichment for the canonical ETS factor family motifs ($p = 1 \times 10^{-129}$; top). Activated peaks show enrichment for consecutive GGAA repeat elements ($p = 1 \times 10^{-878}$; bottom).

(B) Signal tracks for representative repressed binding sites (ENC1 and RAB3GAP2) in SKNMC cells. EWS-FLI1, H3K27ac, and p300 signals for shGFP- or shFLI1-infected cells are shown. The genomic sequence for the EWS-FLI1 binding site near ENC1 is provided (single GGAA).

(legend continued on next page)

organization was induced in mesenchymal stem cells by DNA looping upon expression of EWS-FLI1 (Figure 3H). EWS-FLI1 can therefore act as a pioneer factor and generate active enhancers de novo in mesenchymal stem cells by increasing chromatin accessibility, directing the recruitment of histone methyltransferases and acetyltransferases, and resulting in the establishment of long-range regulatory interactions.

Given that our data point to a direct distal regulatory role for EWS-FLI1 bound GGAA repeats and that variations in repeat size have been proposed as a potential contributor to Ewing sarcoma susceptibility (Beck et al., 2012), we also considered whether EWS-FLI1-bound repeat elements may exhibit length variability. Because Ewing sarcoma displays a 10-fold higher incidence in European compared with African populations, we matched EWS-FLI1-bound GGAA repeats to recent data for variation in microsatellite repeat lengths (Abecasis et al., 2012; Willems et al., 2014). Thirty-six of 244 sites for which variation data were available displayed statistically significant differences between these two groups (25 were longer in Europeans; Table S2). Therefore, EWS-FLI1-bound repeat sites display variability in length between populations and may provide insights into tumor susceptibility.

EWS-FLI1 Directly Represses Targets by Displacing Wild-Type ETS Factors from Mesenchymal Enhancers

We next considered the mechanism by which EWS-FLI1 binding at repressed target sites causes a reduction in p300 occupancy and H3K27ac levels. In contrast to activated sites, repressed sites occupy highly conserved genomic locations (Figure 3B) and contain canonical ETS sequences recognized by a large family of transcriptional activators. Consistently, many of the sites correspond to enhancers that are active in multiple mesenchymal cell types, including primary MSCs, differentiated osteoblasts, and skeletal muscle, but not in embryonic stem cells or neural progenitors (ENCODE Project Consortium, 2012; Figure 4A).

We hypothesized that wild-type ETS activators might be displaced by EWS-FLI1 at these sites, leading to a disruption of mesenchymal lineage enhancers, thus facilitating the interruption of the mesenchymal differentiation characteristic of Ewing sarcoma. To test this hypothesis, we examined the influence of EWS-FLI1 binding on ETS factor occupancy. We focused on the ETS-related transcription factor ELF1, which has a similar sequence preference as FLI1 and is expressed in A673 and SKNMC cells. We surveyed ELF1 binding in SKNMC cells by ChIP-seq before and after EWS-FLI1 knockdown (Figure 4B; Figure S4A). Depletion of the fusion protein led to a marked increase in ELF1 binding at a substantial subset of EWS-FLI1-repressed enhancers (Figures 4B and 4C; Figure S4B). We also examined a second ETS factor, GABPA, and found that it also localizes to many EWS-FLI1 enhancers after depletion of the fusion protein (Figures S4C and S4D). A combined analysis of ELF1 and GABPA occupancy changes shows that repressed sites may exhibit increases in either transcription factor separately or a gain of both ELF1 and GABPA together after EWS-FLI1 knockdown (Figures S4D and S4E). ETS factors such as ELF1 and GABPA are known to robustly recruit p300, whereas EWS-FLI1 lacks one of the two p300 binding domains contained in wild-type FLI1 and, therefore, has weak p300 recruitment when it does not bind as multimers (Hollenhorst et al., 2011). Therefore, the restoration of wild-type ETS factor binding likely explains the increased histone acetylation and enhancer activity observed at EWS-FLI1 sites upon fusion protein depletion. Our findings suggest that EWS-FLI1 represses this subset of conserved enhancers directly by displacing more active wild-type ETS family members from their native binding sites.

EWS-FLI1-Mediated Chromatin Remodeling Is Associated with Expression Changes in Target Genes Involved in Tumor Survival and Differentiation Pathways

Finally, we sought to address the impact of altered *cis*-regulatory element activity on the transcriptional landscape of Ewing sarcoma. We performed RNA sequencing (RNA-seq) in the Ewing sarcoma lines before and after EWS-FLI1 knockdown. By mapping EWS-FLI1 distal elements to the nearest expressed genes, we observed a strong relationship between changes in enhancer activity and changes in proximal gene expression ($p < 10^{-10}$). We confirmed a subset of regulated gene targets by quantitative RT-PCR (Figure S5A). Activated targets include genes shown previously to have important roles in Ewing sarcoma pathogenesis but for which regulatory mechanisms have yet to be defined, such as *CCND1* (Sanchez et al., 2008), *NKX2-2* (Smith et al., 2006), *EZH2* (Riggi et al., 2008), and *SOX2* (Riggi et al., 2010). We also identified many additional targets of EWS-FLI1, such as *OTX2* (Di et al., 2005), *MAFB* (Vicente-Dueñas et al., 2012), *DEK* (Riveiro-Falkenbach and Soengas, 2010), and *API5* (Morris et al., 2006), which have yet to be implicated in Ewing sarcoma (Tables S3 and S4). Several of these activated targets have established roles as oncogenes in other cellular contexts. In contrast, genes directly repressed by EWS-FLI1 include the known tumor suppressors *ERRFI1* (Duncan et al., 2010), *CABLES1* (Arnason et al., 2013), *IER3* (Sebens Müerköster et al., 2008), and *TGFBI* (Wang et al., 2012) as well as mesenchymal lineage factors such as *SNAI2* (Cobaleda et al., 2007), *TRPS1* (Zhang et al., 2012), and *CD73* (Chamberlain et al., 2007) (Tables S3 and S4).

We hypothesized that direct regulatory targets of EWS-FLI1 might represent attractive therapeutic targets in Ewing sarcoma and, therefore, ranked target genes by combined changes in chromatin and expression (Figure 5B). Several highly ranked genes in this set encode kinases. For example, *PRKCB* encodes protein kinase C-β, whose knockdown has been shown previously to induce apoptosis in Ewing cell lines (Surdez et al., 2012). Another top candidate is *VRK1*, a cell cycle-dependent tyrosine kinase involved in G2-M transition (Valbuena et al., 2011). *VRK1* is proximal to an EWS-FLI1-dependent enhancer that is active in Ewing sarcoma cell lines and primary tumors

(C) Signal tracks for representative activated binding sites (NKX2-2 and NPY1R) as in (B). The genomic sequence for the EWS-FLI1 binding site near NKX2-2 is provided (GGAA repeats). Areas of EWS-FLI1 binding are highlighted in gray. These data suggest that repression and activation of EWS-FLI1 bound sites rely on two distinct chromatin remodeling mechanisms, dictated by the underlying genomic sequence and the differential recruitment of p300.
See also Figure S2.

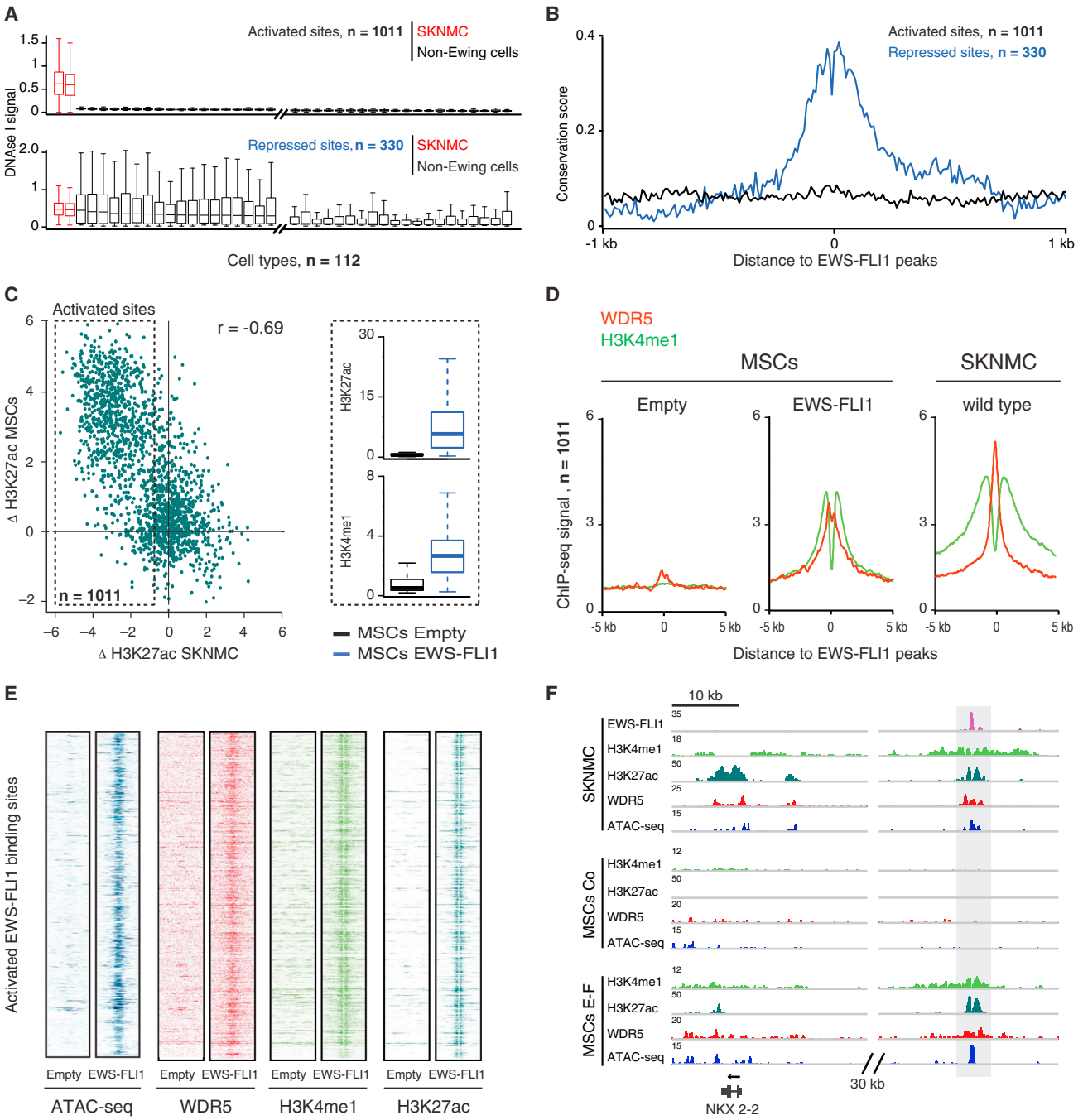

(legend on next page)

and induced de novo by the fusion protein in MSCs (Figure 5C). Chromatin conformation capture (3C) studies confirmed the long-distance interaction between the EWS-FLI1-bound enhancer and the *VRK1* promoter in both SKNMC and A673 cells (see Figures 5D and 5E, respectively).

VRK1 protein expression was confirmed in 15 of 15 primary Ewing sarcoma samples analyzed by immunohistochemistry, which revealed strong VRK1 signals in virtually all cells (Figure 6A; Figure S5B). EWS-FLI1 knockdown markedly reduced VRK1 expression in the cell lines, whereas EWS-FLI1 induction was sufficient to upregulate this kinase in MSCs (Figure 6B; Figure S5C). We directly tested the dependence of Ewing sarcoma cell lines on VRK1 by shRNA knockdown (Figure S5D). The Ewing sarcoma cell lines displayed a high sensitivity to the suppression of this kinase, as indicated by a profound reduction in proliferation and a rapid onset of apoptosis (Figures 6C and 6D; Figures S5E and S5F). In contrast, VRK1 depletion in non-Ewing sarcoma cell lines only moderately decreased proliferation and failed to trigger apoptosis, consistent with recent studies of its function in other tumor models (Kim et al., 2013; Molitor and Traktman, 2013). Finally, injection of VRK1-depleted SKNMC cells immediately after lentiviral infection resulted in a marked decrease in tumor development in vivo (p value $< 10^{-5}$), confirming the critical role of this direct target in sustaining tumor cell proliferation and survival (Figures 6E and 6F). Therefore, de novo induction of enhancers through recognition of GGAA repeats enables EWS-FLI1 to activate genes essential for Ewing sarcoma proliferation and survival (Figure 7).

DISCUSSION

In summary, we have characterized the mechanisms by which a single oncogene reprograms the regulatory and transcriptional landscape of Ewing sarcoma. Through the coordinated analysis of chromatin states at EWS-FLI1 binding sites, we find that the fusion protein is a major determinant of the regulatory activity of a large set of enhancers shared by Ewing cell lines and primary tumors. Depending on the underlying DNA sequence of each binding site, the translocation can either repress its target by displacing more active wild-type transcription factors or activate it by opening chromatin and recruiting chromatin-modifying complexes to genomic regions previously devoid of regulatory function. These different modes of chromatin regulation have robust effects on enhancer activity and on the expression levels of their target genes, including oncogenes, tumor suppressors, and mesenchymal markers with known or candidate roles in Ewing sarcoma.

Genome-wide chromatin profiling indicates that de novo conversion of nonfunctional GGAA repeats into active regulatory elements is the major mechanism of enhancer activation by EWS-FLI1. Binding of EWS-FLI1 to GGAA repeats has been reported previously, and sequences containing at least four GGAA repeats have been shown to favor the binding of EWS-FLI1 as homodimers (Gangwal et al., 2010). In addition, GGAA repeats were the most significant motif in recent binding studies for EWS-ERG (Wei et al., 2010), the second most common chromosomal translocation in Ewing sarcoma, suggesting that similar regulatory mechanisms are shared by Ewing tumors with less frequent fusion partners. We now show that EWS-FLI1 operates as an oncogenic pioneer factor at GGAA repeat sites, mediating a transition from closed to open chromatin and establishing an active enhancer state. Induction of these sites is achieved despite a notable lack of regulatory potential in mesenchymal stem cells, a putative cell of origin of this tumor, or in any other cell or tissue model represented in publically available accessibility data sets (Thurman et al., 2012). EWS-FLI1 expression in mesenchymal stem cells can induce de novo chromatin opening and creation of active enhancers that closely resemble those present in Ewing cells lines and primary tumors. Interestingly, although enhancers are often populated and driven by the binding of multiple collaborative transcription factors, our data suggest that the configuration of EWS-FLI1 as multimers at repeat sites is on its own sufficient to open chromatin and recruit methyltransferase and acetyltransferase activities to generate de novo active regulatory elements. Although it is possible that other DNA binding proteins may become involved in this

Figure 3. EWS-FLI1 Binding Leads to Opening of Chromatin and Recruitment of Chromatin Remodeling Complexes to Induce De Novo Active Enhancers at DNA Repeats Lacking Regulatory Functions in Other Contexts

(A) Box plots for DNaseI signals at activated (top) or repressed (bottom) EWS-FLI1 binding sites across 112 cell lines profiled by ENCODE. SKNMC cells are shown in red.

(B) Conservation scores (PhastCons) in 100 vertebrate species for 2 kb intervals centered on activated or repressed EWS-FLI1 binding sites.

(C) Left: comparison of H3K27ac changes at EWS-FLI1 binding sites after introduction of EWS-FLI1 in MSCs or after EWS-FLI1 depletion in SKNMC cells. Activated EWS-FLI1 binding sites are boxed with a dashed line. Right: box plots of H3K27ac (top) and H3K4me1 (bottom) signal intensities at 1,011 EWS-FLI1-activated sites after introduction of EWS-FLI1 in MSCs (blue) compared with an empty vector control (black). Signals for both enhancer marks are induced significantly following EWS-FLI1 expression.

(D) Composite plots of WDR5 and H3K4me1 signals at activated EWS-FLI1 binding sites in MSCs expressing EWS-FLI1 or infected with an empty vector. Signals in SKMNC cells are shown on the right for comparison.

(E) Heatmaps depicting signals for ATAC-seq, WDR5, H3K4me1, and H3K27ac at activated binding sites as in (C), either from empty vector-infected or EWS-FLI1-expressing MSCs. The rows show ATAC-seq 2 kb regions and WDR5, H3K4me1, and H3K27ac 10 kb regions centered on EWS-FLI1 peaks.

(F) Signal tracks for EWS-FLI1, H3K4me1, H3K27ac, WDR5, and ATAC-seq at the NKX2-2 locus in SKNMC cells and MSCs expressing EWS-FLI1 (E-F) or empty vector control (Co). EWS-FLI1 expression in MSCs leads to nucleosomal rearrangement, WDR5 recruitment, and de novo deposition of both enhancer marks, H3K4me1 and H3K27ac, recapitulating the open active chromatin architecture of SKNMC cells.

(G and H) 3C qPCR analysis of long-distance interactions between the NKX2-2 promoter and the corresponding EWS-FLI1-bound distal regulatory element in SKNMC (G) and primary mesenchymal stem cells (H). A strong interaction is present between the distal regulatory element and the promoter of NKX2-2 in SKNMC cells. No significant interaction is observed in MSCs until the introduction of EWS-FLI1 leads to DNA looping (H) to produce a conformation similar to SKNMC cells. The human NKX2-2 locus is depicted above each graph. The x axes represent distances (kilobases) from the NKX2-2 promoter. A red arrow denotes the HindIII fragment serving as anchor, and black and blue arrows denote the analyzed HindIII fragments. P, promoter; E, enhancer. Error bars represent SD.
See also Figure S3.

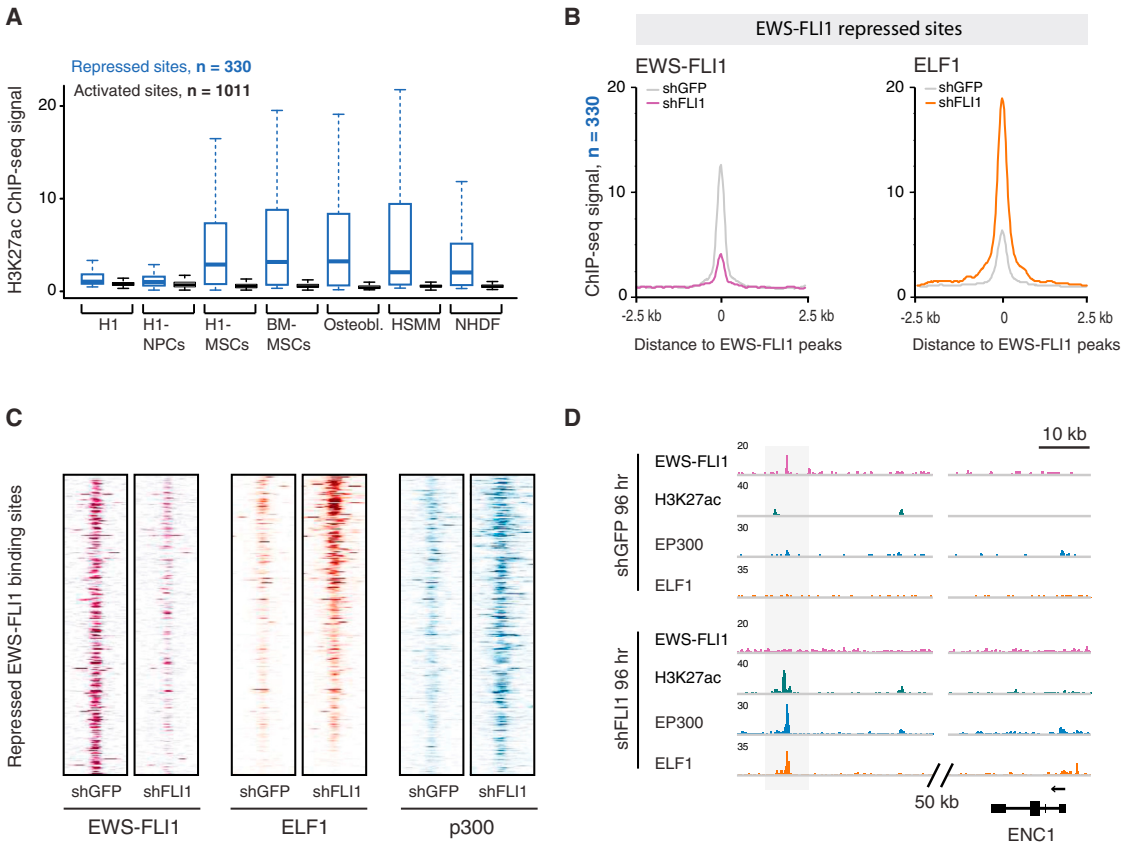

Figure 4. EWS-FLI1 Represses Conserved Distal Regulatory Elements by Displacing Endogenous Wild-Type ETS Factors

(A) Box plots of H3K27ac signal intensities at distal elements corresponding to EWS-FLI1 peaks (repressed sites, blue; activated sites, black) in H1 embryonic stem cells, H1-derived neural progenitor cells (NPCs), H1-derived MSCs, bone marrow-derived MSCs (BM-MSCs), osteoblasts (Osteobl.), skeletal muscle myoblasts (HSMM), and dermal fibroblasts (NHDF). Repressed EWS-FLI1-bound distal elements in Ewing sarcoma are active in normal mesenchymal cell types but not in H1 ES cells or H1-derived NPCs.

(B) Composite plots showing EWS-FLI1 (left) and ELF1 (right) signal intensities for 330 repressed EWS-FLI1 binding sites upon EWS-FLI1 depletion in SKNMC cells.

(C) Heatmaps depicting signals for EWS-FLI1, ELF1, and p300 at the same repressed sites. The rows show 2 kb regions centered on EWS-FL1 peaks. ELF1 binding is observed at many of these sites upon EWS-FLI1 depletion.

(D) Signal tracks for EWS-FLI1, H3K27ac, p300, and ELF1 at the ENC1 locus in SKMNC cells. After EWS-FLI1 depletion, ELF1 binding leads to p300 recruitment and enhancer activation. Areas of EWS-FLI1 binding are highlighted in gray.

See also Figure S4.

process, the absence of pre-existing regulatory signals suggests that the fusion protein is the driving event for these striking changes in the chromatin state.

The activity of EWS-FLI1 at GGAA repeats is also remarkable for the fact that these genomic locations are not conserved and do not appear to have regulatory functions in all other cellular contexts tested. The ENCODE DNase I hypersensitivity data analyzed here include profiles for endothelial and hematopoietic lines that express high levels of endogenous FLI1, but there is no evidence of open chromatin at repeats bound by EWS-FLI1. The large-scale conversion of GGAA repeats to critical tumor-specific regulatory elements may, therefore, be a property specific to the oncogenic fusion protein. These findings raise the intriguing possibility that other aberrant transcriptional mediators in cancer may also operate as pioneer factors to establish critical regulatory elements at DNA sites without normal regulatory activity or evolutionary conservation. It is worth noting that, although the lack of conservation of repeat sites suggests limitations for modeling EWS-FLI1-mediated events in other organisms, the ability of the fusion protein to act as a pioneer factor may result in the activation of different GGAA repeats near locations corresponding to EWS-FLI1 binding sites in humans. It is therefore possible that appropriately localized GGAA repeats may allow EWS-FLI1 to regulate some fraction of its target gene repertoire in other species (Tanaka et al., 2014).

In contrast to activation, the direct repression of enhancers by EWS-FLI1 occurs at nonrepeat canonical ETS binding sites that display strong evolutionary conservation and regulatory activity in other cell types. In particular, DNase I hypersensitivity and H3K27ac activation marks show that these sites often represent active enhancers in cells of mesenchymal origin. Therefore, the known ability of EWS-FLI1 to block differentiation into mesenchymal lineages may be, in large part, mediated by the direct repression of enhancers that control normal developmental

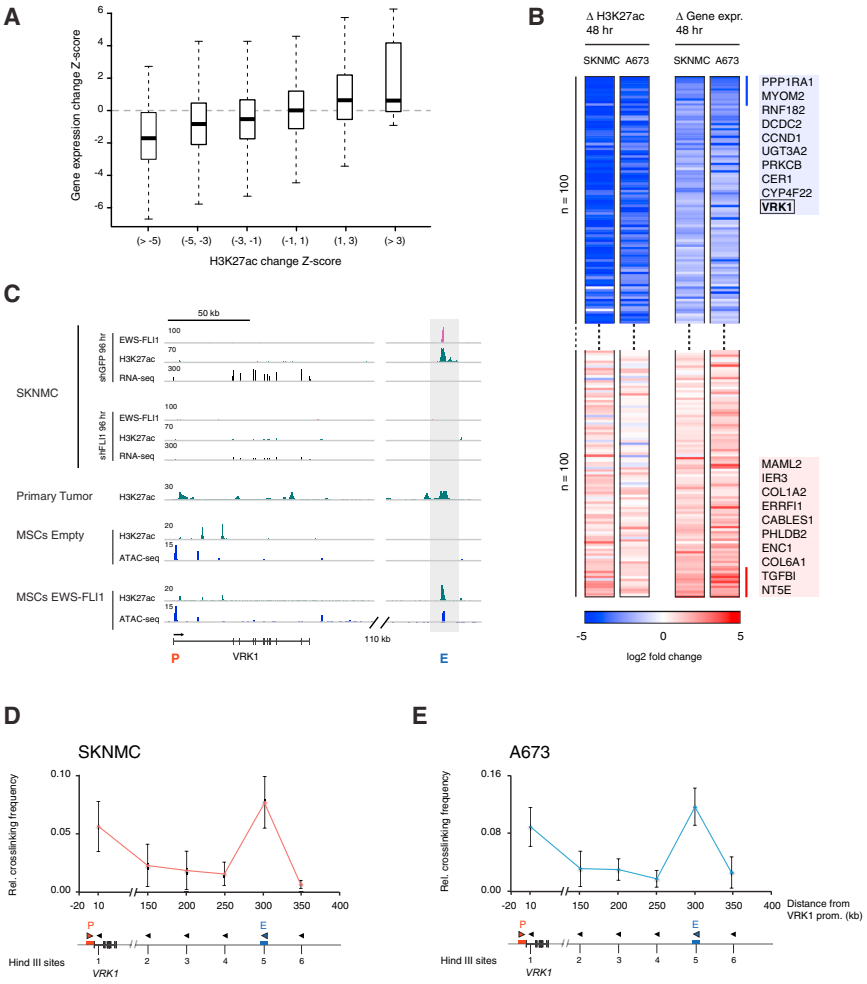

Figure 5. Combined Analysis of Epigenetic States, Transcriptional Changes, and Chromatin Conformation Identifies the Tyrosine Kinase VRK1 as a Direct EWS-FLI1 Target Gene in Ewing Sarcoma

(A) Box plots showing *Z* scores for gene expression changes versus *Z* scores for H3K27ac chromatin changes after EWS-FLI1 knockdown in SKNMC and A673 cells (48 hr). *Z* scores provide a measure of effect, size, and consistency between cell lines. The nearest expressed genes in SKNMC and A673 cells were assigned to each binding site.

(B) Heatmaps depicting fold changes in H3K27ac and gene expression in A673 and SKNMC Ewing cells after EWS-FLI1 knockdown (48 hr). Genes were ranked by the combined significance of H3K27ac and gene expression changes (average *Z* score). The top 100 activated or repressed enhancer binding sites and genes are shown in the heatmap, and the top 10 annotated genes are listed on the right.

(C) Track signals for EWS-FLI1, H3K27ac, and RNA-seq in SKNMC after EWS-FLI1 depletion (96 hr) identify an active regulatory element distal to VRK1 (top). The same enhancer element is present in primary Ewing tumors (center) and is generated de novo by EWS-FLI1 expression in MSCs (bottom).

(D and E) 3C qPCR analysis of long-distance interactions between the VRK1 promoter and the corresponding EWS-FLI1-bound distal regulatory element in SKNMC (D) and A673 cells (E). The human VRK1 locus is depicted below each graph. The x axes represent distances (kilobases) from the VRK1 promoter. The red arrow denotes the HindIII fragment serving as anchor, and black and blue arrows denote the analyzed HindIII fragments. Error bars represent SD.

See also Figure S5 and Tables S3 and S4.

pathways. The finding that this mode of chromatin regulation by EWS-FLI1 is the result of competition and displacement of more active wild-type ETS factors is particularly relevant for alterations in this large gene family and may also extend to other transcription factors with multiple roles in development and cancer.

Our data are consistent with a strong relationship between changes in chromatin states at enhancers and changes in transcriptional activity of proximal genes. In particular, among the affected genes, we found oncogenes and tumor suppressors with known and potential roles in Ewing sarcoma. Given the limitations of analytical methods for assigning enhancers to the nearest genes, we also sought to establish a direct physical interaction between activated enhancer sites and target promoters. Our 3C experiments for both the *NKX2-2* and *VRK1* loci demonstrate that GGAA repeats with active chromatin marks physically interact with target promoters by looping and, therefore, appear to operate as typical enhancers to regulate gene expression. These findings suggest that the genome-wide associations identified in our study may be mediated by similar mechanisms and that enhancer looping is a critical process in Ewing sarcoma pathogenesis.

The mechanisms identified in this study allow EWS-FLI1 to have a major impact on chromatin states and to establish the oncogenic regulatory landscape of Ewing sarcoma. Given the proposed origin of Ewing sarcoma from mesenchymal stem cells, the combined induction of oncogenic drivers and repression of mesenchymal differentiation pathways can serve powerful dual functions in oncogenesis. The characterization of chromatin states and remodeling events in additional tumor models may reveal oncogenic addiction pathways and mechanisms that complement those gleaned from genetic and transcriptomic studies of cancer models. This is exemplified by the association between an aberrant distal regulatory element controlling VRK1 expression and the preferential dependency of Ewing sarcoma cells on this cell cycle-dependent kinase. Taken together, these observations suggest that rewiring of transcriptional regulatory mechanisms by superimposed epigenetic programs can drive functional tumor dependencies and underscore the potential of these analyses for understanding tumor biology and identifying therapeutic targets.

EXPERIMENTAL PROCEDURES

Cell Culture and Primary Tumors

Primary Ewing sarcoma specimens and mesenchymal stem cells were collected with approval from the Institutional Review Boards of Massachusetts

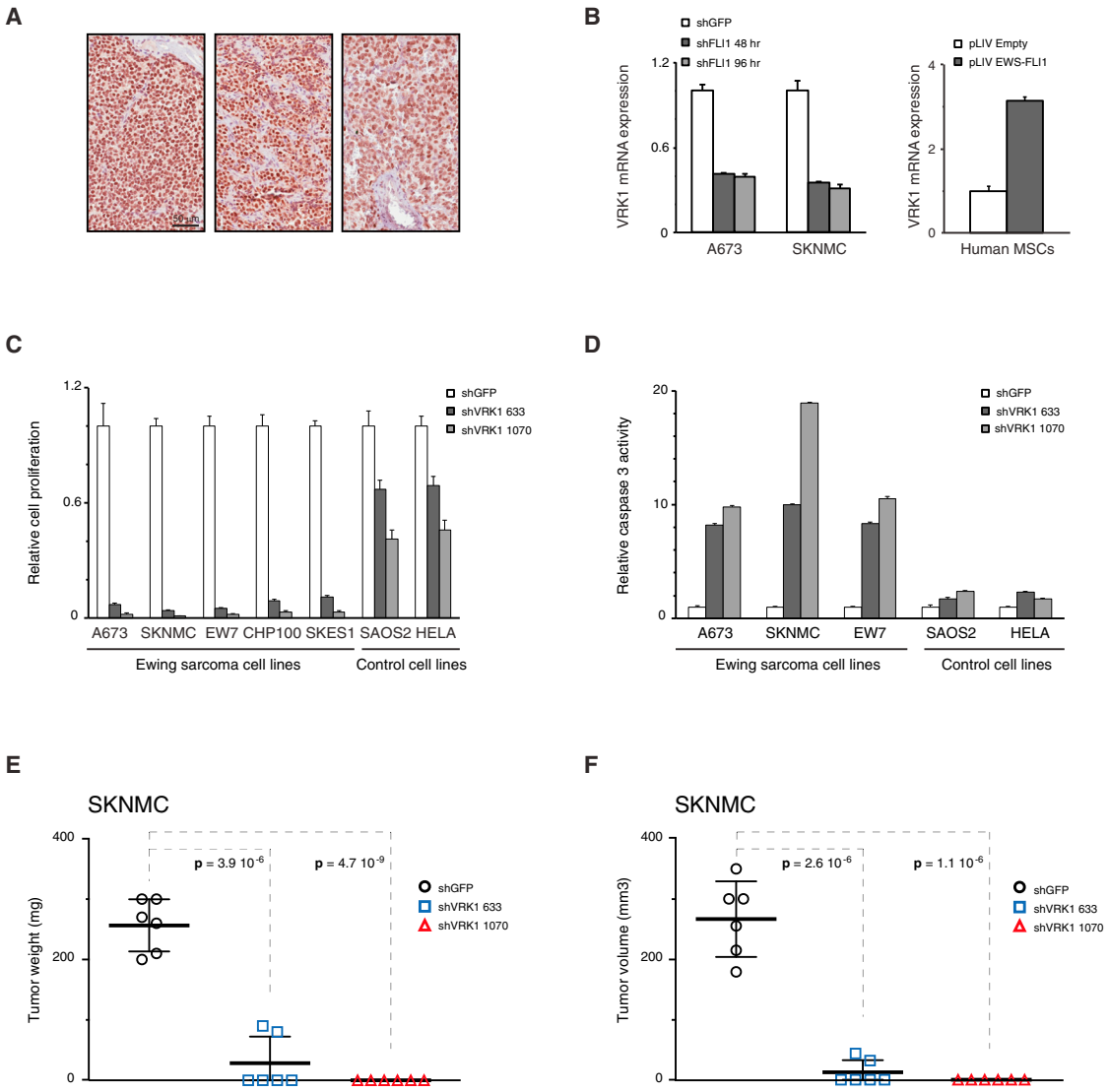

Figure 6. VRK1 Is Highly Expressed in Primary Ewing Sarcoma, and Its Depletion Strongly Reduces Tumor Proliferation and Survival In Vitro and In Vivo

(A) VRK1 is expressed in the majority of Ewing sarcoma cells, as assessed by immunohistochemistry of primary tumors (magnification, 400×; scale bar, 50 μM).

(B) Left: VRK1 mRNA expression in A673 and SKNMC cells after EWS-FLI1 depletion (shFLI1) compared with the control (shGFP). Right: VRK1 mRNA expression in MSCs after introduction of EWS-FLI1 (pLIV EWS-FLI1) compared with control cells (pLIV empty). Error bars represent SD.

(C and D) Proliferation rates (C) and relative apoptosis (D) of a panel of tumor cell lines after VRK1 knockdown compared with the control (shGFP). Error bars represent the SD of three replicates. Ewing sarcoma cells display a selective high sensitivity toward VRK1 depletion compared with Saos-2 (osteosarcoma) and HeLa cells.

(E and F) VRK1 depletion markedly reduces tumor growth in immunocompromised mice, as assessed by tumor weight (E) and volume (F) 3 weeks after subcutaneous injection of control or VRK1-depleted SKNMC cells. Error bars represent SD.

General Hospital and Centre Hospitalier Universitaire Vaudois (CHUV, University of Lausanne). Samples were deidentified prior to our analysis. Primary Ewing sarcoma tumors used for chromatin profiling were confirmed to express the EWS-FLI1 translocation by RT-PCR. Primary pediatric mesenchymal stem cells were cultured in Iscove's modified Dulbecco's medium containing 10% fetal calf serum (FCS) and 10 ng/ml platelet-derived growth factor BB (PeproTech), as described previously (Riggi et al., 2010). The Ewing sarcoma cell lines A673, SKNMC, CHP100, SKES1, and EW7 as well as the SaOS2, HeLa, and 293T cell lines were obtained from the ATCC and grown in RPMI medium containing 10% FCS at 37°C with 5% CO_2. Cells were maintained between a density of 5 × 10^5 cells/ml and 2 × 10^6 cells/ml and split every 3–4 days according to ATCC recommendations.

Real-Time Quantitative RT-PCR and Western Blot Analysis

For gene expression assays, cDNA was obtained using a high-capacity RNA-to-cDNA kit (Applied Biosystems). Five hundred nanograms of template total RNA and random hexamers was used for each reaction. Real-time PCR amplification was performed using fast SYBR Green Master Mix (Life Technologies) and specific PCR primers in a 7500 Fast PCR instrument (Applied Biosystems). Relative quantification of each target, normalized to an endogenous control (*GAPDH*), was performed using the comparative Ct method (Applied Biosystems). Error bars indicate SD. Western blotting was performed using standard protocols. Primary antibodies used for Western blotting were polyclonal rabbit anti-FLI1 (Santa Cruz Biotechnology, catalog no. sc-356, 1:500 dilution), polyclonal rabbit anti-VRK1 (Santa Cruz, catalog no. 1F6, 1:500 dilution), and

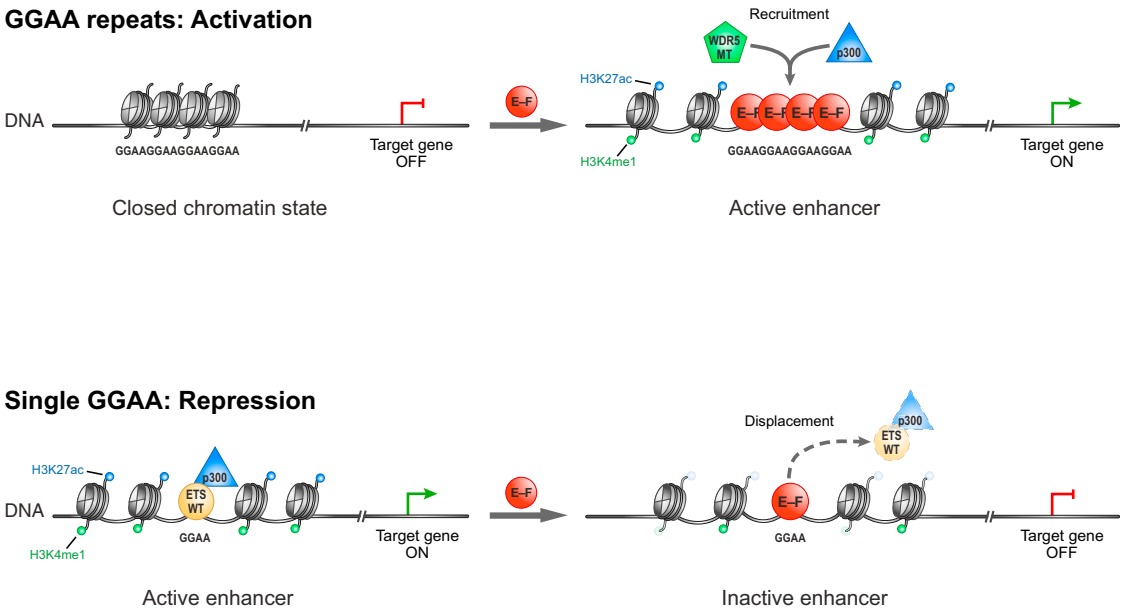

Figure 7. Mechanisms of Enhancer Remodeling Driven by EWS-FLI1

Schematic illustrating the two distinct chromatin remodeling mechanisms underlying EWS-FLI1-divergent transcriptional activity: enhancer induction and activation (top) with recruitment of WDR5 and p300 at GGAA repeats and enhancer repression (bottom) with displacement of endogenous ETS transcription factors and p300 at single GGAA canonical ETS motifs.

monoclonal mouse anti-PARP (Santa Cruz, catalog no. sc-8007, 1:500 dilution). Secondary antibodies were goat anti-rabbit and goat anti-mouse immunoglobulin G-horseradish peroxidase-conjugated (Bio-Rad, 1:20,000 dilution). Membranes were developed using Western Lightning Plus-ECL enhanced chemiluminescence substrate (PerkinElmer) and visualized using photographic film.

EWS-FLI1 Depletion and Expression Experiments

For knockdown experiments, the following lentiviral shRNAs were obtained from the RNAi Consortium in the pLKO.1 vector: *FLI1* (TRCN0000005322) and *VRK1* (TRCN0000197134 and TRCN0000002133). The pLKO.1 shGFP control target sequence was GCAAGCTGACCCTGAAGTTCAT. The *EWS-FLI1* type 1 expression plasmid has been described previously (Riggi et al., 2010). Lentiviruses were produced using standard protocols. Briefly, cDNA coding or shRNA plasmids were cotransfected with *GAG/POL* and *VSV* plasmids into 293T packaging cells using FugeneHD (Roche) to produce the virus. Viral supernatant was collected 72 hr after transfection and concentrated by ultracentrifugation using an SW41Ti rotor (Beckman Coulter Genomics) at 28,000 rpm for 120 min. RNA was extracted at the indicated time points using the QIAGEN RNeasy kit following the manufacturer's instructions.

Proliferation and Apoptosis Assays

Viable cell lines were plated in three to four replicates in 24-well tissue culture plates. For proliferation assays, cells were titrated to allow log phase growth for a period of 5 days prior to readout (5,000 cells/well). Cell proliferation and apoptosis were measured using the CellTiter-Glo luminescent cell viability assay and Caspase-Glo 3/7 luminescent assay, respectively (Promega), as described by the manufacturer. Endpoint luminescence was measured on a SpectraMax M5 plate reader (Molecular Devices). The data displayed are representative of two similar experiments.

In Vivo Tumorigenesis Assay

For in vivo experiments 2×10^6 SKNMC cells were infected with shRNA hairpins targeting either *GFP* (control) or *VRK1* gene sequences, harvested immediately after lentiviral infection, and injected subcutaneously into six nonobese diabetic/severe combined immune deficiency mice for each condition. Mice were monitored daily for tumor development and sacrificed 3 weeks later, when tumor weight and volume were assessed. Animal experiments were performed with approval from the Institutional Animal Care and Use Committee at Massachusetts General Hospital.

ChIP Assays

ChIP assays were carried out on A673, SKNMC, and MSCs cultures of approximately 3–10 $\times$ 10^6 cells per sample and per epitope, following the procedures described previously (Ku et al., 2008; Mikkelsen et al., 2007). Primary human tumors were processed as described previously (Aiden et al., 2010). Because of limited amounts of material, three of four available frozen primary tumors were analyzed for each chromatin mark. In brief, chromatin from formaldehyde-fixed cells was fragmented to a size range of 200–700 bases with a Branson 250 sonifier. Solubilized chromatin was immunoprecipitated with antibodies against H3K4me3 (Millipore), H3K27me3 (Millipore), H3K27ac (Abcam, Active Motif), H3K4me1 (Abcam), FLI1 (Santa Cruz, catalog no. sc-356), ELF1 (Santa Cruz, catalog no. sc-631), GABPA (Santa Cruz, catalog no. sc-22810), p300 (Santa Cruz, catalog no. sc-585) or WDR5 (Bethyl Laboratories, catalog no. A302-429A). Antibody-chromatin complexes were pulled down with protein G-Dynabeads (Life Technologies), washed, and then eluted. After crosslink reversal, RNase A, and proteinase K treatment, immunoprecipitated DNA was extracted with the Min-Elute PCR purification kit (QIAGEN). ChIP DNA was quantified with Qubit. ChIP DNA samples were used to prepare sequencing libraries, and ChIP DNA and input controls were sequenced with the Hi-Seq Illumina genome analyzer.

ACCESSION NUMBERS

The data accompanying this paper have been deposited into GEO under accession number GSE61953.

SUPPLEMENTAL INFORMATION

Supplemental Information includes Supplemental Experimental Procedures, five figures, and four tables and can be found with this article online at http://dx.doi.org/10.1016/j.ccell.2014.10.004.

AUTHOR CONTRIBUTIONS

N.R., B.K., B.E.B., and M.N.R. designed the study and wrote the manuscript. N.R., B.K., S.G., G.B., E.W.B., N.E.R., and E.B.C. performed the experiments. E.R., V.T., M.A., and M.N.R. conducted bioinformatic analyses. O.O. built initial constructs and validated them in vitro. M.L.S., A.P., A.F.D.S.L., D.T.T., F.J.H., P.G.N., and I.S. provided necessary reagents and conceptual advice.

ACKNOWLEDGMENTS

We thank R. Issner, X. Zhang, C. Epstein, N. Shoresh, T. Durham, H. Whitton, M. Hatan, and the Broad Genome Sequencing Platform for technical assistance and L. Gaffney and L. Solomon for help with illustrations. B.K. was supported by a NIH T32 Training Grant (HL007574-30) and a St. Baldrick's fellowship. N.R. was supported by the Swiss National Science Foundation (Grant P3SMP3_148408), by the Nuovo Soldati Foundation, and by the Fond de perfectionnement CHUV. This work was supported by the Howard Hughes Medical Institute (to B.E.B. and MNR), by the National Human Genome Research Institute (ENCODE U54 HG006991) (to B.E.B.), by Hyundai Hope on Wheels (to M.N.R.), and by the Burroughs Wellcome Fund (to B.E.B., M.N.R, and D.T.T.). M.N.R., D.T.T., and V.D. receive research support from Affymetrix. B.E.B. is a scientific advisory board member for Syros Pharmaceuticals and a founder and scientific advisor for HiFiBio SAS.

Received: March 18, 2014
Revised: July 14, 2014
Accepted: October 6, 2014
Published: October 30, 2014

REFERENCES

Abecasis, G.R., Auton, A., Brooks, L.D., DePristo, M.A., Durbin, R.M., Handsaker, R.E., Kang, H.M., Marth, G.T., and McVean, G.A.; 1000 Genomes Project Consortium (2012). An integrated map of genetic variation from 1,092 human genomes. Nature *491*, 56–65.

Aiden, A.P., Rivera, M.N., Rheinbay, E., Ku, M., Coffman, E.J., Truong, T.T., Vargas, S.O., Lander, E.S., Haber, D.A., and Bernstein, B.E. (2010). Wilms tumor chromatin profiles highlight stem cell properties and a renal developmental network. Cell Stem Cell *6*, 591–602.

Arnason, T., Pino, M.S., Yilmaz, O., Kirley, S.D., Rueda, B.R., Chung, D.C., and Zukerberg, L.R. (2013). Cables1 is a tumor suppressor gene that regulates intestinal tumor progression in Apc(Min) mice. Cancer Biol. Ther. *14*, 672–678.

Baylin, S.B., and Jones, P.A. (2011). A decade of exploring the cancer epigenome - biological and translational implications. Nat. Rev. Cancer *11*, 726–734.

Beck, R., Monument, M.J., Watkins, W.S., Smith, R., Boucher, K.M., Schiffman, J.D., Jorde, L.B., Randall, R.L., and Lessnick, S.L. (2012). EWS/FLI-responsive GGAA microsatellites exhibit polymorphic differences between European and African populations. Cancer genetics *205*, 304–312.

Bilke, S., Schwentner, R., Yang, F., Kauer, M., Jug, G., Walker, R.L., Davis, S., Zhu, Y.J., Pineda, M., Meltzer, P.S., and Kovar, H. (2013). Oncogenic ETS fusions deregulate E2F3 target genes in Ewing sarcoma and prostate cancer. Genome Res. *23*, 1797–1809.

Chamberlain, G., Fox, J., Ashton, B., and Middleton, J. (2007). Concise review: mesenchymal stem cells: their phenotype, differentiation capacity, immunological features, and potential for homing. Stem Cells *25*, 2739–2749.

Cobaleda, C., Pérez-Caro, M., Vicente-Dueñas, C., and Sánchez-García, I. (2007). Function of the zinc-finger transcription factor SNAI2 in cancer and development. Annu. Rev. Genet. *41*, 41–61.

Delattre, O., Zucman, J., Plougastel, B., Desmaze, C., Melot, T., Peter, M., Kovar, H., Joubert, I., de Jong, P., Rouleau, G., et al. (1992). Gene fusion with an ETS DNA-binding domain caused by chromosome translocation in human tumours. Nature *359*, 162–165.

Di, C., Liao, S., Adamson, D.C., Parrett, T.J., Broderick, D.K., Shi, Q., Lengauer, C., Cummins, J.M., Velculescu, V.E., Fults, D.W., et al. (2005). Identification of OTX2 as a medulloblastoma oncogene whose product can be targeted by all-trans retinoic acid. Cancer Res. *65*, 919–924.

Duncan, C.G., Killela, P.J., Payne, C.A., Lampson, B., Chen, W.C., Liu, J., Solomon, D., Waldman, T., Towers, A.J., Gregory, S.G., et al. (2010). Integrated genomic analyses identify ERRFI1 and TACC3 as glioblastoma-targeted genes. Oncotarget *1*, 265–277.

ENCODE Project Consortium (2012). An integrated encyclopedia of DNA elements in the human genome. Nature *489*, 57–74.

Gangwal, K., Sankar, S., Hollenhorst, P.C., Kinsey, M., Haroldsen, S.C., Shah, A.A., Boucher, K.M., Watkins, W.S., Jorde, L.B., Graves, B.J., and Lessnick, S.L. (2008). Microsatellites as EWS/FLI response elements in Ewing's sarcoma. Proc. Natl. Acad. Sci. USA *105*, 10149–10154.

Gangwal, K., Close, D., Enriquez, C.A., Hill, C.P., and Lessnick, S.L. (2010). Emergent Properties of EWS/FLI Regulation via GGAA Microsatellites in Ewing's Sarcoma. Genes & cancer *1*, 177–187.

Guillon, N., Tirode, F., Boeva, V., Zynovyev, A., Barillot, E., and Delattre, O. (2009). The oncogenic EWS-FLI1 protein binds in vivo GGAA microsatellite sequences with potential transcriptional activation function. PLoS ONE *4*, e4932.

Hollenhorst, P.C., McIntosh, L.P., and Graves, B.J. (2011). Genomic and biochemical insights into the specificity of ETS transcription factors. Annu. Rev. Biochem. *80*, 437–471.

Kadoch, C., and Crabtree, G.R. (2013). Reversible disruption of mSWI/SNF (BAF) complexes by the SS18-SSX oncogenic fusion in synovial sarcoma. Cell *153*, 71–85.

Kaikkonen, M.U., Spann, N.J., Heinz, S., Romanoski, C.E., Allison, K.A., Stender, J.D., Chun, H.B., Tough, D.F., Prinjha, R.K., Benner, C., and Glass, C.K. (2013). Remodeling of the enhancer landscape during macrophage activation is coupled to enhancer transcription. Mol. Cell *51*, 310–325.

Kim, I.J., Quigley, D., To, M.D., Pham, P., Lin, K., Jo, B., Jen, K.Y., Raz, D., Kim, J., Mao, J.H., et al. (2013). Rewiring of human lung cell lineage and mitotic networks in lung adenocarcinomas. Nat. Commun. *4*, 1701.

Ku, M., Koche, R.P., Rheinbay, E., Mendenhall, E.M., Endoh, M., Mikkelsen, T.S., Presser, A., Nusbaum, C., Xie, X., Chi, A.S., et al. (2008). Genomewide analysis of PRC1 and PRC2 occupancy identifies two classes of bivalent domains. PLoS Genet. *4*, e1000242.

Lawrence, M.S., Stojanov, P., Polak, P., Kryukov, G.V., Cibulskis, K., Sivachenko, A., Carter, S.L., Stewart, C., Mermel, C.H., Roberts, S.A., et al. (2013). Mutational heterogeneity in cancer and the search for new cancer-associated genes. Nature *499*, 214–218.

Lee, T.I., and Young, R.A. (2013). Transcriptional regulation and its misregulation in disease. Cell *152*, 1237–1251.

Margueron, R., and Reinberg, D. (2011). The Polycomb complex PRC2 and its mark in life. Nature *469*, 343–349.

Mikkelsen, T.S., Ku, M., Jaffe, D.B., Issac, B., Lieberman, E., Giannoukos, G., Alvarez, P., Brockman, W., Kim, T.K., Koche, R.P., et al. (2007). Genome-wide maps of chromatin state in pluripotent and lineage-committed cells. Nature *448*, 553–560.

Molitor, T.P., and Traktman, P. (2013). Molecular genetic analysis of VRK1 in mammary epithelial cells: depletion slows proliferation in vitro and tumor growth and metastasis in vivo. Oncogenesis *2*, e48.

Morris, E.J., Michaud, W.A., Ji, J.Y., Moon, N.S., Rocco, J.W., and Dyson, N.J. (2006). Functional identification of Api5 as a suppressor of E2F-dependent apoptosis in vivo. PLoS Genet. *2*, e196.

Patel, M., Simon, J.M., Iglesia, M.D., Wu, S.B., McFadden, A.W., Lieb, J.D., and Davis, I.J. (2012). Tumor-specific retargeting of an oncogenic transcription factor chimera results in dysregulation of chromatin and transcription. Genome Res. *22*, 259–270.

Ramakrishnan, R., Fujimura, Y., Zou, J.P., Liu, F., Lee, L., Rao, V.N., and Reddy, E.S. (2004). Role of protein-protein interactions in the antiapoptotic function of EWS-Fli-1. Oncogene *23*, 7087–7094.

Riggi, N., and Stamenkovic, I. (2007). The Biology of Ewing sarcoma. Cancer Lett. *254*, 1–10.

Riggi, N., Cironi, L., Provero, P., Suvà, M.L., Kaloulis, K., Garcia-Echeverria, C., Hoffmann, F., Trumpp, A., and Stamenkovic, I. (2005). Development of Ewing's

sarcoma from primary bone marrow-derived mesenchymal progenitor cells. Cancer Res. *65*, 11459–11468.

Riggi, N., Suvà, M.L., Suvà, D., Cironi, L., Provero, P., Tercier, S., Joseph, J.M., Stehle, J.C., Baumer, K., Kindler, V., and Stamenkovic, I. (2008). EWS-FLI-1 expression triggers a Ewing's sarcoma initiation program in primary human mesenchymal stem cells. Cancer Res. *68*, 2176–2185.

Riggi, N., Suvà, M.L., De Vito, C., Provero, P., Stehle, J.C., Baumer, K., Cironi, L., Janiszewska, M., Petricevic, T., Suvà, D., et al. (2010). EWS-FLI-1 modulates miRNA145 and SOX2 expression to initiate mesenchymal stem cell reprogramming toward Ewing sarcoma cancer stem cells. Genes Dev. *24*, 916–932.

Riveiro-Falkenbach, E., and Soengas, M.S. (2010). Control of tumorigenesis and chemoresistance by the DEK oncogene. Clinical cancer research *16*, 2932–2938.

Roberts, C.W., Galusha, S.A., McMenamin, M.E., Fletcher, C.D., and Orkin, S.H. (2000). Haploinsufficiency of Snf5 (integrase interactor 1) predisposes to malignant rhabdoid tumors in mice. Proc. Natl. Acad. Sci. USA *97*, 13796–13800.

Sanchez, G., Delattre, O., Auboeuf, D., and Dutertre, M. (2008). Coupled alteration of transcription and splicing by a single oncogene: boosting the effect on cyclin D1 activity. Cell Cycle *7*, 2299–2305.

Schwartzentruber, J., Korshunov, A., Liu, X.Y., Jones, D.T., Pfaff, E., Jacob, K., Sturm, D., Fontebasso, A.M., Quang, D.A., Tönjes, M., et al. (2012). Driver mutations in histone H3.3 and chromatin remodelling genes in paediatric glioblastoma. Nature *482*, 226–231.

Sebens Müerköster, S., Rausch, A.V., Isberner, A., Minkenberg, J., Blaszczuk, E., Witt, M., Fölsch, U.R., Schmitz, F., Schäfer, H., and Arlt, A. (2008). The apoptosis-inducing effect of gastrin on colorectal cancer cells relates to an increased IEX-1 expression mediating NF-kappa B inhibition. Oncogene *27*, 1122–1134.

Smith, R., Owen, L.A., Trem, D.J., Wong, J.S., Whangbo, J.S., Golub, T.R., and Lessnick, S.L. (2006). Expression profiling of EWS/FLI identifies NKX2.2 as a critical target gene in Ewing's sarcoma. Cancer Cell *9*, 405–416.

Smith, E., Lin, C., and Shilatifard, A. (2011). The super elongation complex (SEC) and MLL in development and disease. Genes Dev. *25*, 661–672.

Surdez, D., Benetkiewicz, M., Perrin, V., Han, Z.Y., Pierron, G., Ballet, S., Lamoureux, F., Rédini, F., Decouvelaere, A.V., Daudigeos-Dubus, E., et al. (2012). Targeting the EWSR1-FLI1 oncogene-induced protein kinase PKC-β abolishes ewing sarcoma growth. Cancer Res. *72*, 4494–4503.

Tanaka, M., Yamazaki, Y., Kanno, Y., Igarashi, K., Aisaki, K., Kanno, J., and Nakamura, T. (2014). Ewing's sarcoma precursors are highly enriched in embryonic osteochondrogenic progenitors. J. Clin. Invest. *124*, 3061–3074.

Willems, T., Gymrek, M., Highnam, G., The 1000 Genomes Project Consortium, Mittelman, D., and Erlich, Y. (2014). The landscape of human STR variation. Genome Res. Published online August 18, 2014. http://dx.doi.org/10.1101/gr.177774.114.

Thurman, R.E., Rynes, E., Humbert, R., Vierstra, J., Maurano, M.T., Haugen, E., Sheffield, N.C., Stergachis, A.B., Wang, H., Vernot, B., et al. (2012). The accessible chromatin landscape of the human genome. Nature *489*, 75–82.

Torchia, E.C., Jaishankar, S., and Baker, S.J. (2003). Ewing tumor fusion proteins block the differentiation of pluripotent marrow stromal cells. Cancer Res. *63*, 3464–3468.

Valbuena, A., Sanz-García, M., López-Sánchez, I., Vega, F.M., and Lazo, P.A. (2011). Roles of VRK1 as a new player in the control of biological processes required for cell division. Cell. Signal. *23*, 1267–1272.

Vicente-Dueñas, C., Romero-Camarero, I., González-Herrero, I., Alonso-Escudero, E., Abollo-Jiménez, F., Jiang, X., Gutierrez, N.C., Orfao, A., Marín, N., Villar, L.M., et al. (2012). A novel molecular mechanism involved in multiple myeloma development revealed by targeting MafB to haematopoietic progenitors. EMBO J. *31*, 3704–3717.

Visel, A., Rubin, E.M., and Pennacchio, L.A. (2009). Genomic views of distant-acting enhancers. Nature *461*, 199–205.

Wang, N., Zhang, H., Yao, Q., Wang, Y., Dai, S., and Yang, X. (2012). TGFBI promoter hypermethylation correlating with paclitaxel chemoresistance in ovarian cancer. J. Exp. Clin. Cancer Res. *31*, 6.

Wei, G.H., Badis, G., Berger, M.F., Kivioja, T., Palin, K., Enge, M., Bonke, M., Jolma, A., Varjosalo, M., Gehrke, A.R., et al. (2010). Genome-wide analysis of ETS-family DNA-binding in vitro and in vivo. EMBO J. *29*, 2147–2160.

Zhang, Y., Xie, R.L., Gordon, J., LeBlanc, K., Stein, J.L., Lian, J.B., van Wijnen, A.J., and Stein, G.S. (2012). Control of mesenchymal lineage progression by microRNAs targeting skeletal gene regulators Trps1 and Runx2. J. Biol. Chem. *287*, 21926–21935.